Biophysical Journal, Volume 98

Supporting Material

Chemo-mechanical coupling in F_1-ATPase revealed by catalytic site occupancy during catalysis

Rieko Shimo-Kon, Eiro Muneyuki, Hiroshi Sakai, Kengo Adachi, Masasuke Yoshida, and Kazuhiko Kinosita Jr.

SUPPORTING MATERIAL

Chemo-mechanical coupling in F_1-ATPase revealed by catalytic site occupancy during catalysis

Rieko Shimo-Kon, Eiro Muneyuki, Hiroshi Sakai, Kengo Adachi, Masasuke Yoshida, and Kazuhiko Kinosita Jr.

Contents

Materials and Methods

Materials

ATP, AMP-PNP, regular pyruvate kinase (PK) from rabbit muscle and lactate dehydrogenase (LDH) from hog muscle were purchased from Roche (Basel, Switzerland), and ADP and phosphoenolpyruvate (PEP) from Sigma.

The mutant ΔNCβY341W derived from the thermophile *Bacillus* PS3 (1) was expressed in *E. coli* and purified as described (2). Before use, we heat-treated the protein at 65°C for 4 min for further purification and applied the sample to a size exclusion column (Superdex 200 HR10/30, GE Healthcare) equilibrated with 100 mM KPi, pH 7.0, and 2 mM EDTA to remove tightly-bound nucleotides and then to another column with 10 mM MOPS-KOH, pH 7.0, and 100 mM KCl to remove Pi. Bound nucleotide that remained in the final preparation was 0.05-0.10 mol per mol F_1.

Tryptophan-less (W-less) PK was prepared by mutating the single tryptophan in the *Bacillus stearothermophilus* enzyme to phenylalanine. The mutation was introduced to pKH510 (3) using an oligonucleotide 5'-CGGCGCTTCTTTCGTGTACACGCCGAACACA-AGCGCCAGCCG-3'.

Amino-acid analysis

Protein samples were analyzed by Peptide Institute, Inc. (Osaka, Japan) using Hitachi L-8800 amino acid analyzer and Ajinomoto amino acid calibration mixture. Results on minor amino acids or those that are labile to hydrolysis are omitted from Table S1 below. To calculate expected amounts of amino acids in the Table, the expression plasmid for the ΔNCβY341W mutant was sequenced (FASMAC Co., Ltd., DNA sequencing services, Atsugi, Japan) and amino-acid sequence deduced (Table S2).

ATPase activity

ATP hydrolysis activity was measured at 25°C in buffer M (10 mM MOPS-KOH, pH 7.0, 50 mM KCl, 2 mM $MgCl_2$) in the presence of an ATP-regenerating system consisting of indicated (in figure legends) amounts of PEP, PK, NADH and LDH in a thermostatted spectrophotometer (Hitachi U-3300, Tokyo). After adding a desired amount of MgATP (equimolar mixture of ATP and $MgCl_2$) to the assay mixture, reaction was initiated by rapidly mixing F_1 into the assay mixture with a few strokes of a plastic cuvette mixer. The total volume was 1.6 ml. The absorbance decrease at 340 nm was fitted with an exponential plus a constant for the period between 2 and 20 (or 15) s after the start of mixing, and the slope at 3 s was used to calculate the initial activity. The activity of W-less PK estimated under our assay conditions above with ADP as substrate was characterized by the maximal turnover rate (k_{cat}) of 1,700 s^{-1} (assuming a tetramer molecular weight of 250 kDa) and K_m for ADP of 790 μM. Luciferase assay showed that the regeneration system (2.5 mM PEP, 0.25 mg ml^{-1} PK,

0.15 mM NADH, 0.05 mg ml^{-1} LDH) was contaminated by AT(D)P, converted to ATP by PK, at 32±1 nM (n=3), predominantly from NADH. The contamination was taken into account when calculating free [ATP] in samples.

Measurement of tryptophan fluorescence

Fluorescence was measured in a thermostatted spectrofluorometer (Hitachi F-4500, Tokyo) at 25°C, with excitation at 297 nm (slit width 5 nm in Figs. 5 *B* and 7 *B* and 10 nm in others) and emission at 354 nm (width 20 nm). The assay mixture was buffer M containing indicated components. Prior to F_1 addition, we monitored the background fluorescence continuously at 0.1 s intervals. After the intensity reached a steady level, except for a slight decrease due to photobleaching, we added a desired amount of F_1 rapidly as in the ATPase assay above. The total volume was 1.0 ml. The increase in the fluorescence intensity above the background level was attributed to the F_1 tryptophans. When calculating the degree of quenching at long times, the slight photobleaching of the F_1 fluorescence in the absence of nucleotide (gray in Fig. 3 *B*) was taken into account. Quenching at 3 s was estimated by fitting the 2-20 s portion with an exponential plus a constant. The absorbance of 2 mM ATP at 297 nm was 0.040, and we confirmed that 2 mM ATP decreased the fluorescence of N-acetyl-D-tryptophan by only 2.3% (thanks to the horizontal slit system employed for the fluorometer).

Micro equilibrium dialysis

To calibrate the tryptophan quenching signal, we measured nucleotide binding directly by equilibrium dialysis. We used a micro equilibrium dialyzer (Harvard apparatus, Boston, MA) that has three 250-μl chambers separated by RC membranes (cutoff 10 kDa). The first chamber was filled with buffer M containing a desired amount of MgAT(D)P, the second (central) chamber with 470 nM F_1 in buffer M, and the third with buffer M. The dialysis unit was agitated at room temperature for >30 h on a rotary mixer (VMR-3, ASONE Co., Osaka). Nucleotide concentrations in recovered solutions (recovered volumes for the three chambers were 95, 92, and 99% on average) were determined by reverse phase chromatography (ODS-80Ts, Tosoh, Tokyo) using 100 mM KPi, pH 6.8, as solvent. The solution from the central chamber was treated with perchloric acid, neutralized and centrifuged before chromatography; control nucleotide solutions were treated in the same way.

Estimation of site occupancy

The site occupancy estimated from fluorescence quenching was fitted with the simplest phenomenological relation

$$\text{Occupancy} = [S]/([S] + K_{d1}) + [S]/([S] + K_{d2}) + [S]/([S] + K_{d3}) \qquad \text{(S1)}$$

where [S] stands for free nucleotide concentration (ATP, ADP, or AMP-PNP). The major

purpose was to calculate the free nucleotide concentrations in experiments where the occupancy was not monitored directly.

Rotation assay

F_1 was biotinylated as described (4). Rotation of the γ subunit was observed by attaching a magnetic streptavidin-coated bead(s) (nominal diameter 0.711 μm, Seradyn) to the γ-subunit. A flow chamber was constructed of a bottom coverslip coated with Ni-NTA and an untreated top coverslip (5). 600 pM F_1 in buffer A (25 mM KPi, pH 7.0, 2 mM $MgCl_2$) was introduced in the flow chamber and incubated for 10 min. After another round of F_1 infusion, five chamber volumes of buffer M were infused to remove unbound F_1. Streptavidin-coated magnetic beads in buffer M containing 5 mg ml^{-1} BSA were infused and incubated for 30 min. Finally, 10 chamber volumes of buffer M containing 1 mM creatine phosphate, 0.02 mg ml^{-1} creatine kinase (Roche), and a desired amount of MgATP were infused. To re-activate inhibited F_1, beads were rotated with magnetic tweezers (6). Observation and image analysis were made as described (7).

Reaction scheme

In the analyses (global fit) of the data in Figs. 5, 6 and S3 below, we assumed the following simplified kinetics

$$\mathrm{E+S} \underset{k_{\mathrm{off1}}}{\overset{k_{\mathrm{on1}}}{\rightleftarrows}} \mathrm{ES} \qquad \mathrm{ES+S} \underset{k_{\mathrm{off2}}}{\overset{k_{\mathrm{on2}}}{\rightleftarrows}} \mathrm{ESS} \xrightarrow{k_{\mathrm{cat2}}} \mathrm{ES+D}$$
$$\mathrm{ESS+S} \underset{k_{\mathrm{off3}}}{\overset{k_{\mathrm{on3}}}{\rightleftarrows}} \mathrm{ESS^*\ (+D)} \xrightarrow{k_{\mathrm{cat3}}} \mathrm{ESS+Pi} \qquad \text{(S2)}$$

where E stands for F_1 and S the substrate ATP or ADP that remains bound. ESS corresponds to the ATP-waiting (0°) state in Fig. 1. The product D possibly produced in the bi-site pathway (k_{cat2}) represents ADP, but it will soon be converted to S (ATP) by the regeneration system. When a third ATP binds (k_{on3}), D (ADP) is quickly released, leaving the 80° intermediate ESS* which eventually releases Pi to resume the ESS (ATP-waiting) state. Binding of a medium nucleotide to ESS* is considered only in the calculation of occupancy (no effect on catalysis).

With the above scheme, hydrolysis rate V and site occupancy O at steady state (d[ESS]/dt = 0 etc; not the state after the MgADP inhibition sets in) are given by

$$V = \{k_{\mathrm{cat2}}K_{\mathrm{m3}}[\mathrm{S}]^2 + k_{\mathrm{cat3}}[\mathrm{S}]^3\} \,/\, \{K_{\mathrm{m3}}K_{\mathrm{m2}}K_{\mathrm{m1}} + K_{\mathrm{m3}}K_{\mathrm{m2}}[\mathrm{S}] + K_{\mathrm{m3}}[\mathrm{S}]^2 + [\mathrm{S}]^3\} \qquad \text{(S3)}$$

$$O = \{K_{\mathrm{m3}}K_{\mathrm{m2}}[\mathrm{S}] + 2K_{\mathrm{m3}}[\mathrm{S}]^2 + [\mathrm{S}]^3\ \{2 + [\mathrm{S}]/([\mathrm{S}] + K_{\mathrm{d3}})\}\}$$
$$/\ \{K_{\mathrm{m3}}K_{\mathrm{m2}}K_{\mathrm{m1}} + K_{\mathrm{m3}}K_{\mathrm{m2}}[\mathrm{S}] + K_{\mathrm{m3}}[\mathrm{S}]^2 + [\mathrm{S}]^3\} \qquad \text{(S4)}$$

where $K_{mi} = (k_{cati} + k_{offi})/k_{oni}$, i = 1, 2, 3 with $k_{cat1} = 0$, and K_{d3} the dissociation constant for the loose binding to ESS*. For $K_{m1} << K_{m2} << K_{m3} < K_{d3}$, equation S4 reduces to equation S1

where $K_{d1} = K_{m1}$, $K_{d2} = K_{m2}$, and $K_{d3} = K_{d3}$. Purely tri-site operation is obtained by setting $k_{cat2} = 0$. The tri-site case reduces to a Michaelis-Menten form for $[S] > K_{m2}$ if $K_{m3} >> K_{m2}$.

Supporting Results

Effect of Pi

It has been reported for EF_1 that millimolar Pi or sulfate competes with binding of a nucleotide to a high-affinity catalytic site (8). With our ΔNCβY341W mutant of TF_1, Pi, like PEP but to a greater extent, retarded and suppressed binding of nucleotides (Fig. S3). Unlike PEP, Pi also tended to retard MgADP inhibition (Fig. S3 *A* and *C*).

With 5 mM Pi, the site occupancy at 3 s was ~1 around 1 μM ATP (Fig. S3 *D*), similar to the effect of 50 mM PEP, whereas the hydrolysis activity at 3 s was as high as ~half the activity in the absence of Pi (Fig. S3 *C*), compared to the reduction to ~1/10 by 50 mM PEP. To account for the rather high activity without invoking a bi-site mode, half of the F_1 must bind two nucleotides while the rest bind none. In Fig. S2 we show that this is possible in transient kinetics where a high (mM) concentration of Pi initially competes with ATP for the first binding site (but later yields to ATP of which the affinity for that site is much higher): initially most of F_1 binds Pi alone but gradually the Pi is replaced with ATP, and F_1 that has bound ATP binds a second (and third) ATP immediately to engage in tri-site catalysis. The results are gradual increase in the average site occupancy and hydrolysis activity. With a reasonable choice of rate constants we have been able to reproduce qualitatively the data in Fig. S3 around 1 μM ATP.

We directly confirmed that bi-site activity is indeed negligible even at 5 mM Pi, by depleting medium ATP. With 5 mM Pi, simple addition of ΔNC, as in Fig. 7 in the main text, would fail to deplete medium ATP completely, because Pi will also bind to ΔNC, disabling it from binding the medium ATP. We therefore let hydrolysis proceed at 5 mM Pi and 20 μM ATP (to achieve a high occupancy) on a cuvette mixer and, after 3 s, diluted the sample 40-fold into the same solution without ATP. The sudden decrease of [ATP] resulted in almost complete cessation of hydrolysis (Fig. S4 *A*, green), compared to the control where the diluent also contained 20 μM ATP (cyan). To measure ADP release, we repeated the same procedure, except that the final 40-fold dilution was into 2 μM ΔNC (no ATP) to ensure complete removal of diluted ATP. The site occupancy remained ~2 (Fig. S4 *B*, green), close to the value at 3 s in the control (orange), without showing a sign of ADP release: if the enzyme had engaged in bi-site catalysis, the occupancy would have decreased to one. Bi-site activity is thus negligible even in the presence of 5 mM Pi.

Fig. S3 *D* shows that medium Pi also competes with the binding of the third nucleotide. This strengthens our contention that the third site is open to medium nucleotides, including Pi.

ATP hydrolysis accompanies rotation

The hydrolysis activity at low [ATP] is low, and whether hydrolysis accompanies rotation has not been confirmed for ΔNCβY341W. Due to the ΔNC (α-K175A/T176A) mutation, only ~1% of F_1 remains active at steady state. To observe rotation, therefore, we activated inhibited F_1 under a microscope by attaching a streptavidin-coated magnetic bead(s) to the γ subunit and let the bead rotate with magnets (6). The forced rotation often induced spontaneous rotation, which continued for several revolutions before ending up in another inhibited state (Fig. S5 *A*). We selected those events where F_1 rotated relatively fast for more than five free revolutions, and calculated the time-averaged speeds (Fig. S5 *B*). At [ATP] above 2 μM, viscous friction against the beads limited the rotary speed to ~5 revolutions s^{-1}. At lower [ATP], the rotary speed was proportional to [ATP] and commensurate with one third of the hydrolysis rate, as expected for the 120° rotation per ATP scenario. Indeed, we observed clear 120° stepping at 60 nM ATP (Fig. S5 *A*, inset). Hydrolysis and rotation are coupled in ΔNCβY341W, down to at least 60 nM ATP.

At 60 nM ATP, we noticed that F_1 often made a backward 40° substep from an ATP-waiting angle to enter an inhibited state (Fig. S5 *A*, inset). Backward 40° substeps were also observed with wild-type TF_1 at extremely low [ATP], where the back steps tended to lead to a long-lasting irregular behavior (4). Single-molecule observations with Cy3-ATP indicated that a backward 40° substep was often accompanied by the reduction of site occupancy from two to one (9). Premature release of ADP in an ATP-waiting state may direct F_1 into an off-major reaction pathway(s) that starts with a backward substep, rather than forward bi-site rotation that has to wait for the arrival of a next ATP which takes time at low [ATP].

Supporting material Table S1 Amino acid contents of the wild type TF_1 and ΔNCβY341W.

	Wild type		ΔNCβY341W	
	Expected number	Recovery (%) (n = 1)	Expected number	Recovery (%) (n = 4)
Asp	272	98.2	272	94.4± 2.5
Glu	399	97.8	399	92.8 ± 2.2
Gly	273	98.1	273	94.2 ± 2.9
Ala	294	96.8	300	91.5± 2.6
Leu	294	99.8	294	95.3 ± 3.0
Tyr	94	97.3	91	92.4 ± 3.9
Phe	106	98.3	109	92.1 ± 3.0
Lys	149	97.2	146	93.0 ± 2.8
His	94	95.8	94	92.6 ± 3.1
Arg	192	96.5	192	92.6 ± 2.7
Pro	145	99.1	145	95.1 ± 2.6
weighted average		97.9		93.5 ± 2.7

Results of amino-acid analyses are expressed as percentages of the expected values calculated from the extinction coefficient of ε_{280nm} = 154,000 $M^{-1}cm^{-1}$.

Supporting material Table S2 Amino-acid sequence of the ΔNCβY341W mutant of TF_1.

α subunit

```
1          11         21         31         41
MSIRAEEISA LIKQQIENYE SQIQVSDVGT VIQVGDGIAR AHGLDNVMSG  50
ELVEFANGVM GMALNLEENN VGIVILGPYT GIKEGDEVRR TGRIMEVPVG 100
EALIGRVVNP LGQPVDGLGP VETTETRPIE SRAPGVMDRR SVHEPLQTGI 150
KAIDALVPIG RGQRELIIGD RQTGAASVAI DTIINQKDQN MISIYVAIGQ 200
KESTVRTVVE TLRKHGALDY TIVVTASASQ PAPLLFLAPY AGVAMGEYFM 250
YKGKHVLVVY DDLSKQAAAY RELSLLLRRP PGREAYPGDI FYLHSRLLER 300
AAKLSDAKGG GSLTALPFVE TQAGDISAYI PTNVISITDG QIFLQSDLFF 350
SGVRPAINAG LSVSRVGGAA QIKAMKKVAG TLRLDLAAYR ELEAFAQFGS 400
DLDKATQAKL ARGARTVEVL KQDLHQPIPV EKQVLIIYAL TRGFLDDIPV 450
EDVRRFEKEF YLFLDQNGQH LLEHIRTTKD LPNEDDLNKA IEAFKKTFVV 500
SQ                                                     502
```

β subunit

```
-11        -1
MHHHHHHHHH H
1          11         21         31         41
MTRGRVIQVM GPVVDVKFEN GHLPAIYNAL KIQHKARNEN EVDIDLTLEV  50
ALHLGDDTVR TIAMASTDGL IRGMEVIDTG APISVPVGEV TLGRVFNVLG 100
EPIDLEGDIP ADARRDPIHR PAPKFEELAT EVEILETGIK VVDLLAPYIK 150
GGKIGLFGGA GVGKTVLIQE LIHNIAQEHG GISVFAGVGE RTREGNDLYH 200
EMKDSGVISK TAMVFGQMNE PPGARMRVAL TGLTMAEYFR DEQGQDVLLF 250
IDNIFRFTQA GSEVSALLGR MPSAVGYQPT LATEMGQLQE RITSTAKGSI 300
TSIQAIYVPA DDYTDPAPAT TFSHLDATTN LERKLAEMGI WPAVDPLAST 350
SRALAPEIVG EEHYQVARKV QQTLQRYKEL QDIIAILGMD ELSDEDKLVV 400
HRARRIQFFL SQNFHVAEQF TGQPGSYVPV KETVRGFKEI LEGKYDHLPE 450
DAFRLVGRIE EVVEKAKAMG VEV                              473
```

γ subunit

```
1          11         21         31         41
MASLRDIKTR INATKKTSQI TKAMEMVSTS KLNRAEQNAK SFVPYMEKIQ  50
EVVANVALGA GGASHPMLVS RPVKKTGYLV ITSDRGLAGA YNSNVLRLVY 100
QTIQKRHACP DEYAIIVIGR VGLSFFRKRN MPVILDITRL PDQPSFADIK 150
EIARKTVGLF ADGTFDELYM YYNHYVSAIQ QEVTERKLLP LTDLAENKQR 200
TVYEFEPSQE ECLDVLLPQY AESLIYGALL DAKASEHAAR MTAMKNATDN 250
ANELIRTLTL SYNRARQAAI TQEITEIVAG ANALQ                  285
```

The sequences above have been deduced from the DNA sequence of the expression plasmid.

The numbering scheme starts with Met-1 that is absent in the expressed wild-type subunits or α and γ subunits of HC95 (not confirmed with ΔNCβY341W; expressed HC95 β contains the first Met at position -11). Underlines show mutations introduced in HC95 mutant that we regard as wild type for rotation assay, and double underlines show additional mutations in ΔNCβY341W mutant. The sequence of the γ subunit here is slightly different from the published sequence that contains 283 residues rather than 285 residues above (10). The γ-S107C/I210C mutations referred to in the main text are γ-S109C/I212C in the revised sequence above.

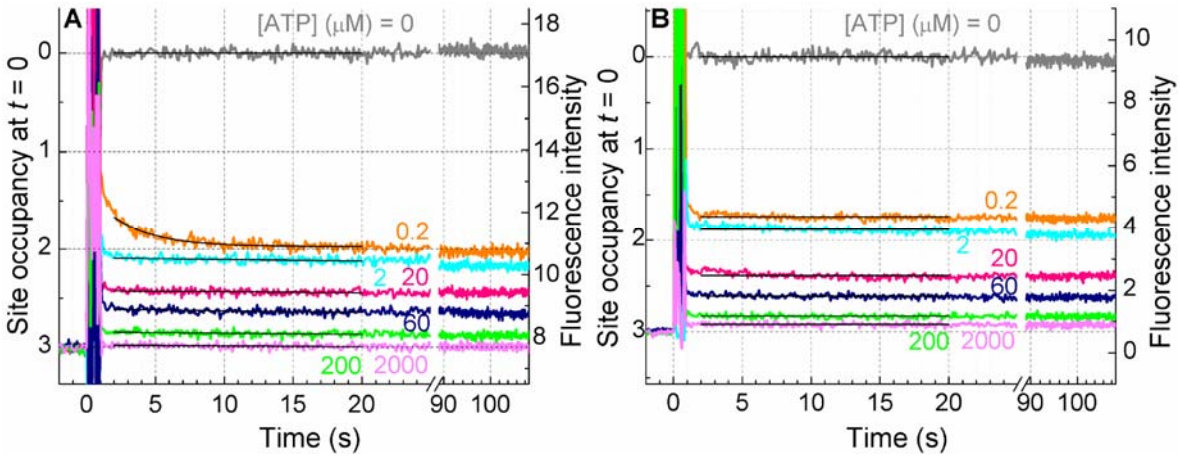

Supporting material Figure S1 Time courses of fluorescence quenching in the presence (*A*) and absence (*B*) of an ATP regeneration system. 19 nM F_1 was added at time 0 to buffer M with 1.0 mM PEP and 0.5mg ml^{-1} W-less PK (*A*) or to buffer M alone (*B*), each containing ATP at the indicated concentration. The W-less PK used in *A* was of higher purity than that in Fig. 3 *B* in the main text, resulting in the lower base line and lower noise.

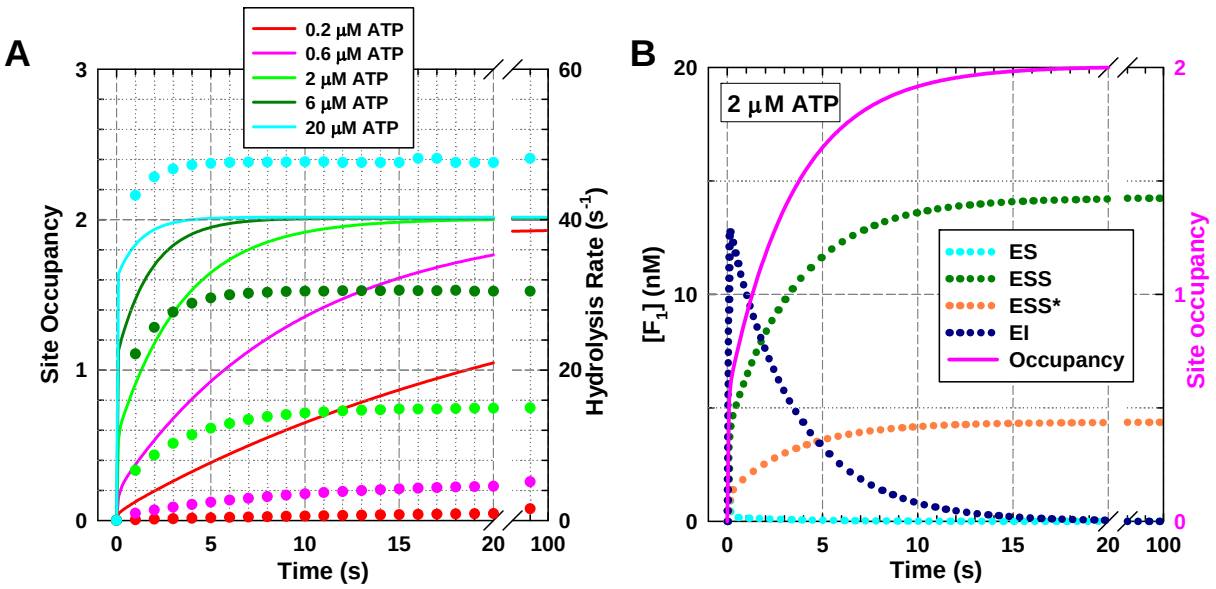

Supporting material Figure S2 Possible kinetics of site occupancy and hydrolysis activity with Pi as competitive inhibitor. (*A*) Calculated time courses of catalytic site occupancy (solid curves) and instantaneous hydrolysis rate (dotted curves) in the presence of 5 mM Pi and indicated [ATP]. (*B*) Changes in the concentrations of enzyme (F_1) species binding different nucleotides at 2 µM ATP and 19 nM F_1 in the presence of 5 mM Pi.

The scheme we assume here is the following. We include, in scheme (S2) in Methods above, the first reaction below that represents competitive binding of the inhibitory Pi (shown as I) to the first catalytic site, and neglect k_{cat2} in scheme (S2):

$$\mathrm{E} + \mathrm{I} \underset{k_{\mathrm{off}}^{\mathrm{I}}}{\overset{k_{\mathrm{on}}^{\mathrm{I}}}{\rightleftarrows}} \mathrm{EI} \qquad \mathrm{E} + \mathrm{S} \underset{k_{\mathrm{off1}}}{\overset{k_{\mathrm{on1}}}{\rightleftarrows}} \mathrm{ES} \qquad \mathrm{ES} + \mathrm{S} \underset{k_{\mathrm{off2}}}{\overset{k_{\mathrm{on2}}}{\rightleftarrows}} \mathrm{ESS}$$

$$\mathrm{ESS} + \mathrm{S} \underset{k_{\mathrm{off3}}}{\overset{k_{\mathrm{on3}}}{\rightleftarrows}} \mathrm{ESS}^{*} \; (+\mathrm{D}) \xrightarrow{k_{\mathrm{cat3}}} \mathrm{ESS} + \mathrm{Pi}$$

As in Methods, E stands for F_1 and S the substrate ATP (or ADP produced by catalysis). The product Pi is negligible compared to I (added Pi). The product D (ADP) is assumed to be immediately converted back to S (ATP) by a regeneration system (this is untrue under our experimental conditions with the limited amount of PK, but we chose this assumption here to simplify the reaction scheme; inclusion of PK and PEP in the above scheme does not change the results significantly). Reaction kinetics was calculated with Reactor version 1.6 (made by Laszlo Oroszi and Andras Der, Biological Research Center of the Hungarian Academy of Sciences) with the initial conditions of [E] = 19 nM, [I] = 5 mM, [S] = [ATP] as indicated in the figure, and the parameter values: $k_{on}^{I} = 10^4$ $M^{-1}s^{-1}$, $k_{off}^{I} = 1$ s^{-1} (increasing k_{on}^{I} and k_{off}^{I} beyond these values while keeping their ratio constant does not significantly alter the results), $k_{on1} = 10^7$ $M^{-1}s^{-1}$, $k_{off1} = 0$ s^{-1} (increasing k_{off1} has no appreciable effect as long as $k_{off1} <$

k_{on1}[S]), $k_{on2} = 10^7$ $M^{-1}s^{-1}$, $k_{off2} = 0$ s^{-1} (no appreciable effect as long as $k_{off2} < k_{on2}$[S]), $k_{on3} = 10^7$ $M^{-1}s^{-1}$, $k_{off3} = 0$ s^{-1} (no appreciable effect up to 1 s^{-1}), and $k_{cat3} = 64$ s^{-1}. Under these conditions, most of the enzyme is either inhibited (EI) or actively engaging in tri-site catalysis (ESS or ESS*), as seen in panel *B*. The one-nucleotide species ES is virtually absent. Thus, the time-dependent site occupancy is given, essentially, by (0×[EI] + 2×[ESS] + 2×[ESS*])/E_0.

The kinetics of simple competitive inhibition for a single-site enzyme (the first two reactions in the above scheme, with the addition of a finite k_{cat1} not shown in the scheme) can be solved in a closed form and leads to the following general conclusions (which can be inferred without solving the differential equations): (i) the approach to the steady state (where [ES] and [EI] no longer change with time) is very slow under the conditions [S] >> K_m, [I] >> $K_d^I = k_{off}^I/k_{on}^I$, because free enzyme E needed for the exchange of ES and EI is virtually absent under these conditions; (ii) if k_{on}^I[I] > k_{on}[S], then most of the enzyme is inhibited at the beginning, the inhibited fraction being given by k_{on}^I[I] / (k_{on}^I[I] + k_{on}[S]); and (iii) eventually EI changes to ES, albeit very slowly, if [S]/K_m > [I]/K_d^I. When all these three conditions are met, the activity of the enzyme very slowly rises from zero to an almost fully active value. The parameters chosen for the simulation above satisfy these conditions: (i) [S] = [ATP] >> $K_{m1} = 0$, [I] = 5 mM >> K_{d1}^I = 0.1 mM; (ii) k_{on}^I[I] = 50 s^{-1} > k_{on1}[ATP] = 20 s^{-1} for 2 μM ATP and below; and (iii) [ATP]/K_m >> [I]/K_d^I = 50 for $K_{m1} = 0$.

Note that the scheme above does not include MgADP inhibition, and thus comparison with our experimental data is meaningful only in the initial portion. Also note that, in the case of F_1-ATPase, the inhibitor I may bind to any of the three catalytic sites, and thus the scheme above where I binds only to the first site is an oversimplification. The major purpose of this calculation is to show, qualitatively, that significant tri-site activity can emerge at low occupancy if transient inhomogeneity (coexistence of active and inhibited F_1) is introduced by a competitive inhibitor.

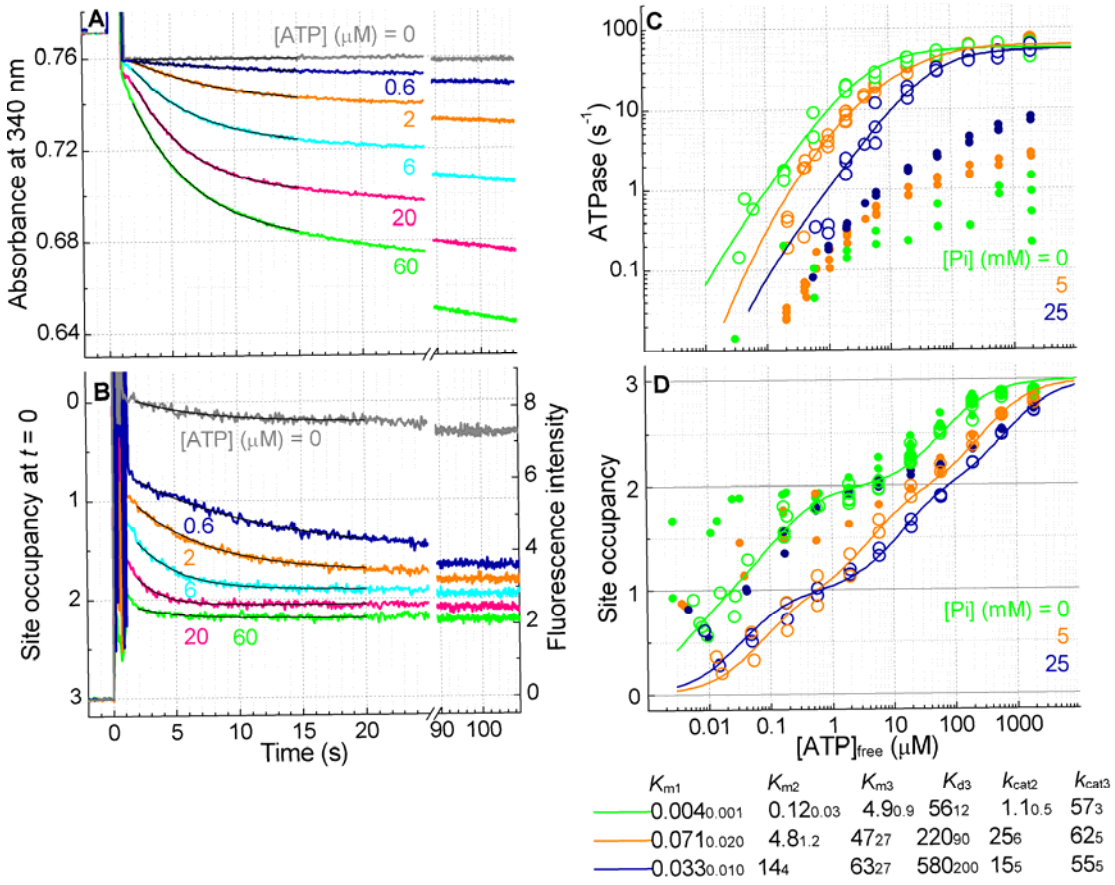

Supporting material Figure S3 Effect of Pi on binding and hydrolysis of ATP. (*A*) Time courses of ATP hydrolysis at 5 mM Pi. 47 nM F_1 was added at time 0 to a regenerating system consisting of 1.0 mM PEP, 0.5 mg ml^{-1} regular PK, 0.15 mM NADH and 0.05 mg ml^{-1} LDH. (*B*) Time courses of nucleotide binding at 5 mM Pi. 19 nM F_1 was added to buffer M without an ATP regenerating system. (*C*) Summary of hydrolysis activities at indicated [Pi]. Open symbols at 3 s and closed symbols at 100-300 s. 5-90 nM F_1 in 1.0 mM PEP, 0.5 or 0.7 mg ml^{-1} regular PK, 0.15 mM NADH and 0.05 mg ml^{-1} LDH. (*D*) Catalytic site occupancies at indicated [Pi]. Open symbols at 3 s and closed symbols at 100 s. Data at 0 mM Pi are reproduction of Fig. 4 *B* (1.0 mM PEP included). PEP was absent at 5 and 25 mM Pi (addition of 1.0 mM PEP did not significantly alter the results). Unquenched fluorescence of ΔNCβY341W was 12% higher at 25 mM Pi, for an unknown reason. Lines are global fit with equations S3 and S4, with parameter values shown at bottom.

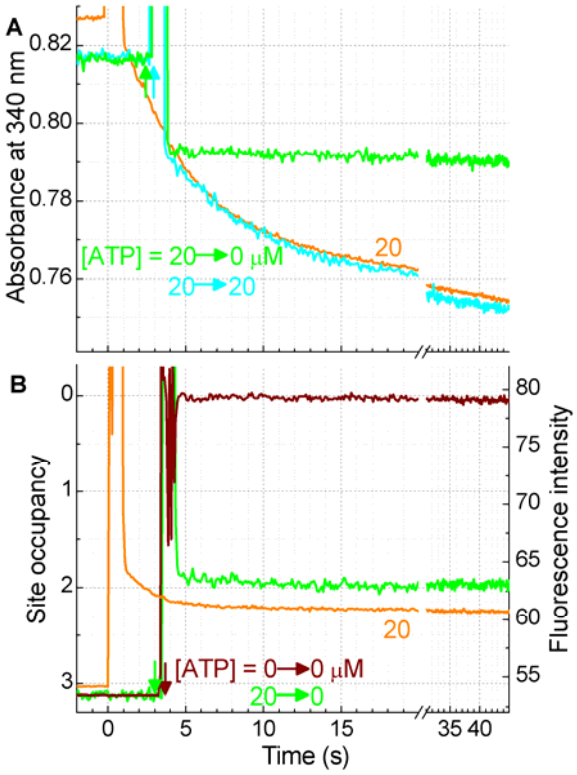

Supporting material Figure S4 Time courses of hydrolysis and ADP release after ATP depletion in the presence of 5 mM Pi. (*A*) Hydrolysis. In green and cyan, 1.9 μM ΔNCβY341W was mixed, at time 0, with 20 μM ATP, 5 mM Pi, 1.0 mM PEP, 1 mg ml^{-1} W-less PK, 0.15 mM NADH and 0.05 mg ml^{-1} LDH in buffer M to start hydrolysis on a cuvette mixer. After 3 s (arrows), the mixer was plunged into 39 volumes of the same solution, except [PK] = 0.5 mg ml^{-1} for both and [ATP] = 0 for green, to monitor hydrolysis activity. Final [ΔNCβY341W] = 47 nM. Orange is a control where 47 nM ΔNCβY341W was directly added to 20 μM ATP at time 0. (*B*) ADP release. In green and brown, 1.9 μM ΔNCβY341W was mixed on a cuvette mixer with 20 μM ATP (0 for brown), 5 mM Pi, 1.0 mM PEP and 1 mg ml^{-1} W-less PK at time 0. After 3 s (arrows), the mixer was plunged into 39 volumes of 2 μM ΔNC (for complete ATP depletion), 5 mM Pi (0 for green, but see below), 1.0 mM PEP and 0.5 mg ml^{-1} W-less PK. Final [PK] was 0.53 mg ml^{-1}, resulting in the slight shift of the base line (the left-hand scale applies to the portions after ~5 s. Final [ΔNCβY341W] = 47 nM. In green, to set final [Pi] to 5 mM but not to pre-expose ΔNC to Pi, a drop of 500 mM Pi was placed separately on the mixer and plunged simultaneously; an indistinguishable result was obtained when the Pi drop was omitted (to not inhibit ΔNC at all) and Pi added at 12 s (not shown). Orange is a control where 47 nM ΔNCβY341W was directly added to 20 μM ATP, 5 mM Pi and 1.0 mM PEP (the right-hand scale does not apply).

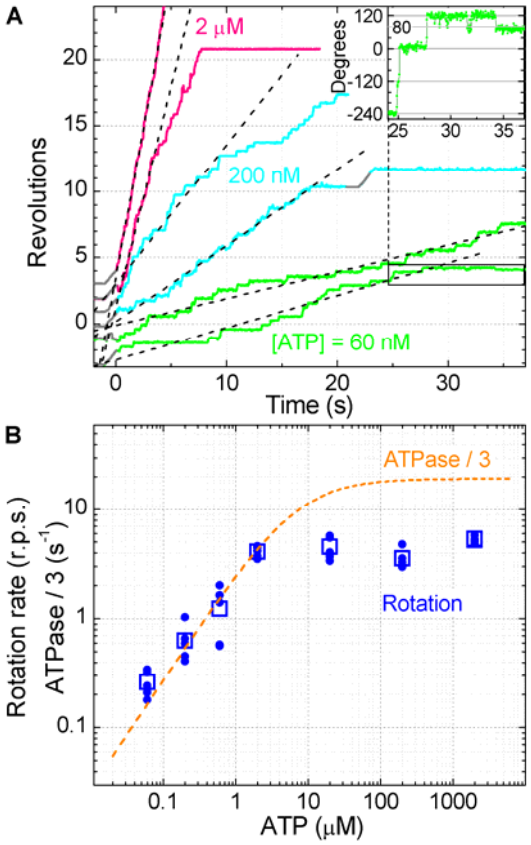

Supporting material Figure S5 Rotation of ΔNCβY341W. (*A*) Time courses of rotation in buffer M. A magnetic bead(s) attached to the γ subunit was rotated by one turn with magnets between -1 to 0 s (gray); spontaneous rotation followed in successful cases, as shown. Dashed lines indicate the portions from which the rotation rate in *B* was estimated. Inset, magnification of the boxed portion. (*B*) [ATP] dependence of the time-averaged rotation rate. Blue dots show individual rates for >5 consecutive revolutions and squares their average. Orange line, one third of the ATPase activity in Fig. 4 *A* in the main text.

Supporting material References

1. Ono, S., K. Y. Hara, J. Hirao, T. Matsui, H. Noji, et al. 2003. Origin of apparent negative cooperativity of F_1-ATPase. *Biochim. Biophys. Acta.* 1607:35-44.
2. Adachi, K., H. Noji, and K. Kinosita, Jr. 2003. Single-molecule imaging of rotation of F_1-ATPase. *Methods Enzymol.* 361:211-227.
3. Sakai, H. 2005. Mutagenesis of the active site lysine 221 of the pyruvate kinase from *Bacillus stearothermophilus*. *J. Biochem.* 137:141-145.
4. Sakaki, N., R. Shimo-Kon, K. Adachi, H. Itoh, S. Furuike, E. et al. 2005. One rotary mechanism for F_1-ATPase over ATP concentrations from millimolar down to nanomolar. *Biophys. J.* 88:2047-2056.
5. Itoh, H., A. Takahashi, K. Adachi, H. Noji, R. Yasuda, et al. 2004. Mechanically driven ATP synthesis by F_1-ATPase. *Nature.* 427:465-468.
6. Hirono-Hara, Y., K. Ishizuka, K. Kinosita, Jr., M. Yoshida, and H. Noji. 2005. Activation of pausing F_1 motor by external force. *Proc. Natl. Acad. Sci. U S A.* 102:4288-4293.
7. Yasuda, R., H. Noji, M. Yoshida, K. Kinosita Jr., and H. Itoh. 2001. Resolution of distinct rotational substeps by submillisecond kinetic analysis of F_1-ATPase. *Nature.* 410:898-904.
8. Bulygin, V. V., and Y. M. Milgrom. 2007. Studies of nucleotide binding to the catalytic sites of *Escherichia coli* βY331W-F_1-ATPase using fluorescence quenching. *Proc. Natl. Acad. Sci. U S A.* 104:4327-4331.
9. Adachi, K., K. Oiwa, T. Nishizaka, S. Furuike, H. Noji, et al. 2007. Coupling of rotation and catalysis in F_1-ATPase revealed by single-molecule imaging and manipulation. *Cell.* 130:309-321.
10. Ohta. S., M. Yohda, M. Ishizuka, H. Hirata, T. Hamamoto, et al. 1988. Sequence and over-expression of subunits of adenosine triphosphate synthase in thermophilic bacterium PS3. *Biochim. Biophys. Acta.* 933:141-155.